Optics Communications 475 (2020) 126208

Contents lists available at ScienceDirect

Optics Communications

journal homepage: www.elsevier.com/locate/optcom

A scalable two-dimensional moving electric lattice on a chip for polar molecules

Bin Wei, Hengjiao Guo, Yabing Ji, Tao Yang, Shunyong Hou *, Jianping Yin

State Key Laboratory of Precision Spectroscopy, East China Normal University, Shanghai 200062, PR China

ARTICLE INFO

Keywords:
2D electric lattice
Molecular chip
Stark deceleration

ABSTRACT

Cold atoms and polar molecules have long been candidates for the implementation of quantum information processing. Although many schemes of two-dimensional (2D) moving optical or magnetic lattices have been proposed for atomic shift register, little work has been done on 2D electric lattice for molecular shift register, mainly due to the complexity of molecular energy level structures as well as the challenge to build micropotentials that are scalable, smoothly moving and accurately controlled. Here we present a design of chip-based 2D electric lattice for molecular shift register capable of scaling and controlling, which mainly consists of arrays of equidistant gold electrodes for generating a moving electric lattice. Our theoretical analysis and trajectory calculations, based on the polar molecules ammonia-D3 (ND_3) and methylidyne radical (CH), show explicitly that the 2D lattice is able to directly slow down arrays of polar molecules from supersonic speeds to a standstill over a distance of a few centimeters, and then hold them for a certain time or shift them back in a smooth manner. Besides, it also enables decelerating and trapping of the two molecular species simultaneously, which contributes to the understanding towards new phenomena such as novel quantum mechanical collisions and cold chemistry.

1. Introduction

Quantum computer (QC) based on quantum mechanical systems has attracted much attention for its ability of solving classically intractable computational problems. Neutral particles such as cold atoms and polar molecules are promising candidates for implementation of quantum information processing (QIP) [1], because they have exquisite coherence properties and their coherent evolution can be precisely controlled in micropotentials, which allow for interfacing their qubit degrees of freedom with solid-state systems. To date, the primary way to create registers of atoms is the optical lattice, which produces arrays of potential wells and helps achieving large-scale quantum entanglement [2–4]. However, 2D optical lattice is generated by interfering laser beams and thus has limitations in the design flexibility and producing arbitrary trap geometries. Also, the spacing of lattice arrays is typically half of the optical wavelength, which is too short for addressing and manipulating the atoms. As an alternative, 2D magnetic lattices on chips [5] for atoms can overcome some of these limitations and enable trapping and manipulating atoms with a high degree of design flexibility.

Compared to the rapid progress in the atomic shift register, little work has been done in molecular shift register, mainly due to the complexity of molecular energy level structures as well as the challenge to build moving micropotentials. Recently, Meijer group demonstrated the first one-dimensional (1D) moving electric lattice on a chip [6,7]. Merkt group realized a 1D moving electric lattice for Rydberg atoms on a printed circuit board [8]. The disadvantage of the scalability due to the 1D moving electric lattice has become major concern in the quest for an implementation of QC. Most recently we proposed a scalable chip-based 2D electric lattice for cold polar molecules [9], but its micropotentials are stationary such that it is not suitable for a molecular shift register. Here, we propose a 2D moving electric lattice on a chip for polar molecules in consideration of the following reasons: (i) a 2D moving electric lattice is a natural extension of its counterparts of 2D moving optical (or magnetic) lattices, and it has some special advantages in accurately controlling neutral particles; (ii) it offers an innovative access to arrays of cold molecules and enables smoothly shuttling arrays of cold molecular packets back and forth, which allows it to act as a molecular shift register for quantum computing; (iii) the 2D moving lattice permits simultaneous deceleration and trapping of two molecular species, which might pave the way for sympathetic cooling of two molecular species as well as the cold collision chemistry [10,11].

2. Design and operation principle

It seems easy to build a 2D moving electric lattice by combining a number of 1D electric lattice arrays, however, the edge effect of

* Corresponding author.
E-mail address: syhou@lps.ecnu.edu.cn (S. Hou).

https://doi.org/10.1016/j.optcom.2020.126208
Received 3 January 2020; Received in revised form 25 April 2020; Accepted 1 May 2020
Available online 22 June 2020

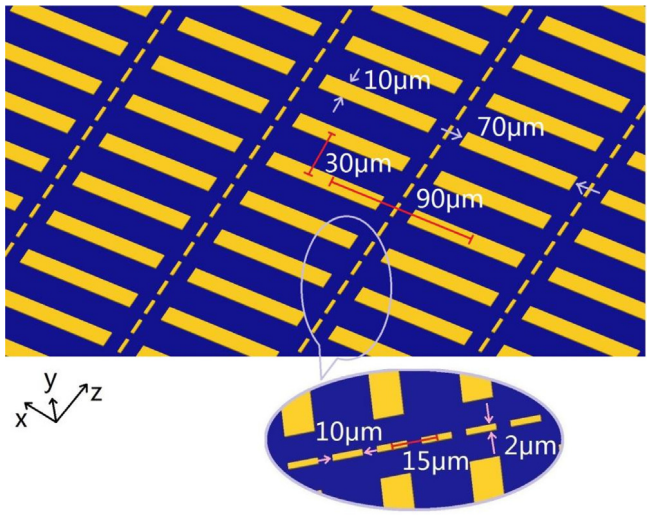

Fig. 1. Schematic of the 2D moving electric lattice for polar molecules as well as the geometric features of the electrodes. Molecular packets captured by the lattice propagate over arrays of big electrodes along the z-direction. In our defined coordinate system, the y-axis is normal to the chip surface and the z-axis is parallel to the propagation direction of the molecular packets.

the electric fields can destroy the micropotentials when these lattices are moving closer to each other. By utilizing arrays of elaborate intermediate electrodes to separate each 1D lattice, the edge effect can be mitigated and a 2D electric lattice can be formed. The next challenge is to make the 2D lattice move smoothly. Initially, no matter how the voltages were applied to these electrodes in our design, the edge effect between adjacent arrays would affect these micropotentials when the 2D lattice was moving. Not until the lattice electrodes and the intermediate electrodes were respectively applied with alternating voltages at an appropriate phase difference that a 2D electric lattice can be set up and move smoothly, which is illustrated in Fig. 1.

As in Fig. 1, the 2D moving electric lattice consists of arrays of equidistant gold electrodes with a thickness of 1 μm, which are deposited onto a glass substrate. The big (or small) electrodes are divided into six sets, where the electrodes in each set along x-axis are connected together through thin wires on the back of the chip. To avoid each set of electrodes crossing each other, more than one dielectric layer is required for the electrode tips that are connected to their corresponding power source respectively. Each big electrode is 10-μm-wide and 70-μm-long, spaced by the center-to-center distances of 30 μm and 90 μm with respect to the neighboring ones in the z- (longitudinal) and x- (transverse) direction, respectively. The voltages for each set of big electrodes are given by $\pm U_1(1+\cos(\omega t+\varphi_n))$, with specific positive (negative) potential for odd (or even) ones and ω being the modulation frequency of the voltage applied on the electrodes. Phase difference of adjacent odd-(even-)numbered electrodes is set to be $\pm 2\pi/3$, therefore odd-(even-)numbered electrodes spaced by two of them are always equal in the magnitude but opposite in sign to the potential applied on them. The adjacent arrays of big electrodes are separated by a chain of small electrodes that play a central role in forming a 2D potential well. Given by the potential of $\pm U_2\cos(\omega t+\varphi_m)$ and phase difference of $\pm 2\pi/3$ between adjacent odd-(even-)numbered one, each small electrode is 2-μm-wide and 10-μm-long, with a center-to-center distance of 15 μm along the z-direction.

Under these settings, a 2D electric lattice is formed in the vicinity of the chip and can move smoothly over the big electrodes in z-direction. For a given frequency ω, the minima of these potential wells travel with a constant velocity of $L\omega/(4\pi)$ along the z-direction, where L is the periodicity of potential ($L = 180$ μm in our case). Note that we choose such geometries of the electrodes and the minima of the potential for the convenience of discussion, which are still subject to scaling at a practical basis.

In a charge-free region of space, the electric potential $\Phi(x, y, z)$ can be derived from Laplace's equation. For our designated 2D electric lattice, the solution is given by

$$\begin{aligned}\Phi(x,y,z) = &\sum_{m,n=0}^{\infty} A_{mn}\exp(-y\sqrt{(mk_x x)^2+(nk_z z)^2}) \\ &\times[\cos(mk_x x)\cos(nk_z z)] \\ &+\sum_{m,n=0}^{\infty} B_{mn}\exp(-y\sqrt{(mk_x x)^2+(nk_z z)^2})[\cos(mk_x x)\sin(nk_z z)],\end{aligned} \tag{1}$$

where $k_x = 4\pi/L$, $k_z = 2\pi/L$ and L is the periodicity of potential. The coefficients A_{mn} and B_{mn} can be determined as follows. The fields are calculated using numerical methods that take into account the finite

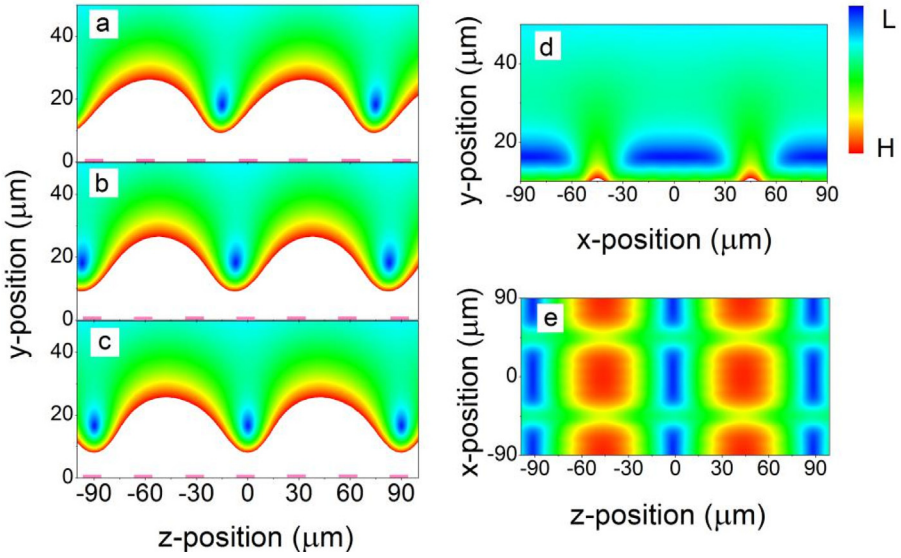

Fig. 2. Subpanels (a)–(c) display three snapshots of electric field strength at three selected time, calculated using Eqs. (1) and (2). Subpanels (d) and (e) indicate the electric field strength contour in the x-y plane and the x-z plane through the minima of the potential wells, respectively. For each site the length scale along the z-direction is about five times longer than that along the x- or y-direction. Color bar labels H and L represent high and low electric fields, respectively.

widths and lengths of the electrodes, and are obtained along the z-axis in the vicinity of the electrodes' surface. By calculating the Fourier transform along these lines in the z-direction, Fourier components can be obtained. We choose $n = 1$ and 3 to create quadrupole potentials in the longitudinal direction. In order to sufficiently reproduce the electric fields above the chip, the value of m is taken account of up to 7. By solving a set of equations obtained by comparing each Fourier component with Eq. (1), the coefficients A_{mn} and B_{mn} in Eq. (1) can be determined. This method for determining the coefficient of an electric field expression is similar to Refs. [12,13]. As long as the electric potential is constrained, the electric field strength is given by

$$|\vec{E}| = \sqrt{\left(\frac{\partial \Phi}{\partial x}\right)^2 + \left(\frac{\partial \Phi}{\partial y}\right)^2 + \left(\frac{\partial \Phi}{\partial z}\right)^2}. \tag{2}$$

And then the force between the polar molecules and the fields can also be derived from the following expression [12]

$$\begin{pmatrix} F_x \\ F_y \\ F_z \end{pmatrix} = -\left(\frac{1}{|\vec{E}|}\frac{dW}{d|\vec{E}|}\right)\begin{pmatrix} \frac{\partial^2 \Phi}{\partial x^2} & \frac{\partial^2 \Phi}{\partial x \partial y} & \frac{\partial^2 \Phi}{\partial y \partial z} \\ \frac{\partial^2 \Phi}{\partial x \partial y} & \frac{\partial^2 \Phi}{\partial y^2} & \frac{\partial^2 \Phi}{\partial y \partial z} \\ \frac{\partial^2 \Phi}{\partial x \partial z} & \frac{\partial^2 \Phi}{\partial y \partial z} & -\frac{\partial^2 \Phi}{\partial x^2} - \frac{\partial^2 \Phi}{\partial y^2} \end{pmatrix}\begin{pmatrix} \frac{\partial \Phi}{\partial x} \\ \frac{\partial \Phi}{\partial y} \\ \frac{\partial \Phi}{\partial z} \end{pmatrix}. \tag{3}$$

where W is Stark potential. For the ammonia-D3 (ND_3) molecule, Stark potential $W(\vec{E})$ is given by

$$W(\vec{E}) = \pm\sqrt{\left(\frac{W_{inv}}{2}\right)^2 + \left(\mu |E| \frac{MK}{J(J+1)}\right)^2} - \frac{W_{inv}}{2}, \tag{4}$$

where W_{inv} is the zero-field inversion splitting (0.053 cm^{-1} for ND_3), and M, K are the projections of the total angular momentum J on the electric field $\vec{E}$ and along the symmetry axis, respectively. From Eqs. (1) and (2), the electric fields above the surface of the chip are calculated and shown in Fig. 2. Fig. 2(a) – (c) represent the distributions of the electric field strength in the y-z plane at three selected time, respectively. It clearly shows that the potential wells can be shifted over the chip in a continuous manner, while the distance of the potential minima from the chip remains constant. Fig. 2(d) and (e) depict the distributions of the electric field strength in the x-y plane and the x-z plane through the minima of the potential wells, respectively. Fig. 2 justifies that arrays of microtraps (i.e. 2D electric lattice) can be formed and move over the chip, and each site is a true 3D electrostatic potential well for polar molecules in the low-field-seeking states. Note that the distance of the potential minima from the chip is determined by the geometric structure of the lattice and is independent from the voltages applied on the electrodes, which is estimated to be 18 μm above the surface of the chip.

3. Longitudinal and transverse effective traps

The longitudinal motion of molecules relative to the moving potential well center is given by

$$m\frac{d^2 \Delta z}{dt^2} + ma - \overline{F}(\Delta z) = 0, \tag{5}$$

where m is the mass of the molecule, Δz is the instantaneous longitudinal position difference between the molecule and the potential well center, and a is the acceleration of the lattice. $\overline{F}(\Delta z)$ is the average force experienced by molecules in the potential well over one period, which can be obtained from Eqs. (1)–(4). The Stark shift of ND_3 close to the center of the trap is quadratic and thus the restoring force is linearly proportional to displacement. The trap frequency can be estimated by taking the potential well as a harmonic trap with the expression $W_z = k_z \cdot z^2/2$, where $k_z = m\omega_z^2$. When the amplitudes of the voltages U_1 and U_2 applied on the electrodes are both 100 V, the longitudinal trap frequency $f_z = \omega_z/2\pi = 110$ kHz.

The transverse motion of the molecules in the moving potential well is given by

$$m\frac{d^2 x, y}{dt^2} - \overline{F}_{x,y} = 0. \tag{6}$$

Here, the average transverse force $\overline{F}_{x,y} = \int_0^L \frac{F_{x,y}(\varphi_0(t),z)}{L} dz$, with $\varphi_0(t)$ being the time-dependent phase offset and expressed as $\varphi_0(t) = 2\pi \int_0^t \omega(\tau) d\tau$, where $\omega(\tau)$ is the modulation frequency of the voltage applied on the electrodes. The phase space acceptance of an individual trap of the electric lattice for the ND_3 molecule can be obtained from Eqs. (5) and (6), as shown in Fig. 3. Fig. 3(a)–(c) illustrate the phase-stability diagrams in three respective directions with the acceleration of the lattice being zero. The area inside the separatrix indicates the acceptance of the lattice, where molecules are phase-stable. Beyond the separatrix the molecules will be lost since their total energy is larger than the effective potential well. Phase stability ensures that the phase-space density remains constant during the deceleration process.

4. Theoretical analysis and trajectory calculations

To justify the performance of our scheme, 3D numerical calculations that include the processes of deceleration and trapping are carried out with ND_3 molecules in the $|J, KM>=|1,-1>$ state (a low-field-seeking state). The simulation model for the 2D moving electric lattice can be described as below. The time- and position-dependent electric fields of the lattice are calculated using Eqs. (1)–(4). Based on these derived electric fields, the force felt by molecules at any time and location can be obtained using interpolation methods. Nonadiabatic transition loss is not considered in our calculations since the molecules in the lattice are kept away from the minima of the potential wells due to the presence of acceleration. For some molecules this loss can also be suppressed by using an offset magnetic field [14]. Other losses caused by background collision and surface-induced heating are also ignored in our simulation as current vacuum technology and cooling technology ensure reducing these losses [15]. The six dimensional emittance of the incident beam is set to be $[\Delta z \times \Delta v_z] \times [\Delta x \times \Delta v_x] \times [\Delta y \times \Delta v_y] = [500\ \mu m \times 30\ m/s] \times [500\ \mu m \times 10 m/s] \times [40\ \mu m \times 10 m/s]$, where the position and velocity spread are flat in all directions. The input beam contains 7.5×10^6 molecules with initial distribution centered at $z = 0$ μm, $v_z = 340$ m/s, $y = 25$ μm, $v_y = 0$ m/s, and $x = 0$ μm, $v_x = 0$ m/s. The amplitudes of the voltages U_1 and U_2 applied on the electrodes are both set to be 100 V.

Our simulation covers the whole dynamic processes including loading, deceleration and detection. The beam of ND_3 molecules first freely flies at a distance of 5 mm and then is coupled into the electric lattice in the z-direction. The initial frequency of the modulated voltages applied on the electrodes is 3.78 MHz, which matches the central velocity (340 m/s) of the incoming molecular beam. The frequency of the modulated voltages is continuously chirped from 3.78 MHz to 0 Hz in about 0.3 ms, resulting in an acceleration up to 1.16 $\mu m \cdot \mu s^{-2}$ that is about five orders of magnitude larger than the acceleration due to gravity. The temperature of molecules in the lattice is also investigated during the process of deceleration. The temperature T is given in the moving frame by $(3/2)k_B T = (1/2)k_B T_L + k_B T_T$ [16], where T_L and T_T are the corresponding longitudinal and transverse temperatures of the molecular packets and defined by the formula $T_{x,y,z} = m(\Delta v_{x,y,z})^2/8 \ln 2 \cdot k_B$ [17], with m being the mass, $\Delta v_{x,y,z}$ the velocity spread (full width at half maximum), and k_B the Boltzmann constant. Fig. 4(a) shows the temperature of molecules in the lattice as a function of the deceleration distance. The temperature of the packets is monotonously reduced from 15 mK to around 10 mK as they are slowed to a standstill. Note that the temperature of the molecular packets is decreased because the depth of the effective trapping potentials is lowered in the slowing process, as seen in Fig. 4(c) and (d). The interaction between the molecules and electric fields is a conservative force and therefore it cannot really

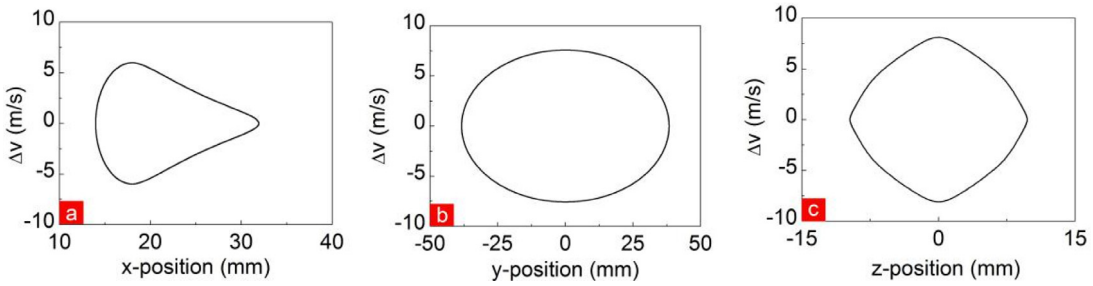

Fig. 3. Phase space acceptance of an individual trap of the moving electric lattice for the ND_3 molecule in three respective directions, with the acceleration of the lattice being zero.

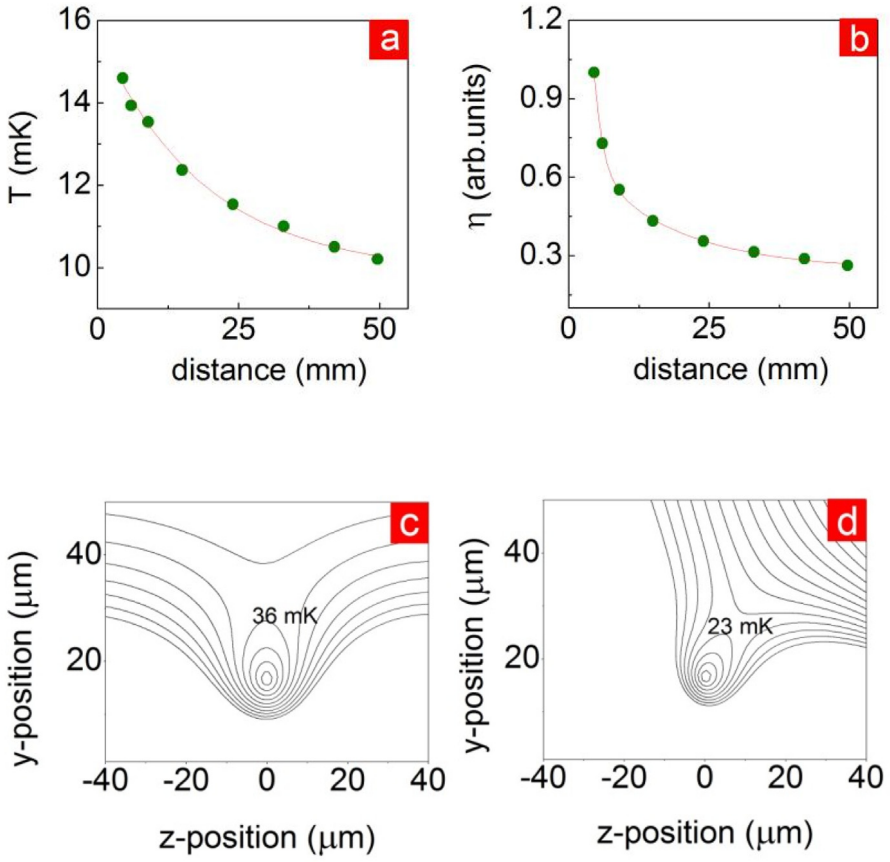

Fig. 4. Temperature of confined molecules in the lattice (a) and the slowing efficiency η (b) as a function of the deceleration distance, together with the fitting curves. Subpanels (c) and (d) show the mechanical potentials of one lattice site in the y-z plane, with accelerations of 0 μm· μs^{-2} and 1.65 μm· μs^{-2}, respectively. The depth of the effective trapping potentials is lowered from 36 mK to 23 mK due to the presence of acceleration. Intervals are respectively 9 mK and 6.8 mK in subpanels (c) and (d).

cool molecules, or increase the phase space density of the molecular packets. The slowing efficiency parameter η is the ratio of the number of molecules ultimately captured in the stationary trap to the number of molecules initially loaded into the moving lattice. From Fig. 4(b) we can observe that it decreases rapidly in the first few millimeters over the chip and the final slowing efficiency of the lattice is near 30% when the ND_3 molecules are brought to a standstill. The mechanical potentials of one site in y-z plane are shown in Fig. 4(c) and (d), with accelerations of 0 μm· μs^{-2} and 1.65 μm· μs^{-2}, respectively. Fig. 4(a) and (b) show that ND_3 molecules are trapped by the lattice, however the depth of the effective potential well is lowered due to the presence of acceleration and thus allows the hottest molecules to escape from the traps. The depth of potential wells in both transverse directions (x- or y-direction) is changed as they propagate along the z-direction. Fortunately this change is very small thus no obvious "wiggling" motion in x- or y-direction will be observed.

Once slowed down to a standstill, the arrays of molecular packets can be held in the lattice at the end of the chip. As illustrated in Fig. 5, these packets can be stably confined in the lattice. The decreasing number density is caused by loss at the phase-space boundaries and, in addition, due to possible numerical imprecision. The inset in Fig. 5 shows the spatial distribution of the molecular packets at the end of the chip. The dots represent the positions of the molecules. The simulated results demonstrate that our proposed 2D moving electric lattice can be used to produce and trap cold molecular samples from a supersonic beam, which is an ideal starting point for the chip-based cold molecular experiments.

5. Applications

5.1. Molecular shift register

The ability of shifting particles back and forth will undoubtedly enhance the functionality of the atomic (molecular) chip devices. Magnetic conveyor belt [18] and 1D optical lattice [19] for transporting ultracold atoms are applicable for some experiments such as optical lattice clock and quantum computation. In 2009, Whitlock et al. introduced a moving 2D magnetic lattice that can act as an atomic shift register [5], which contains a great many of physical qubits for storing and processing quantum information. As an analogue, our proposed 2D electric lattice can be used as a molecular shift register, where polar molecules can be employed as qubits for quantum computing [20–24]. Rather than the magnetic or optical lattices that can only load stationary or slowly moving ultracold samples, our 2D electric lattice enables directly loading and decelerating a fast-moving molecular beam to any final velocity, which greatly simplifies the complexity of the experiment and enhances the number density of molecular packets. In order to justify our scheme for a molecular shift register, trajectory calculations for ND_3 molecules are performed with the same input parameters used in previous section.

A pulsed supersonic ND_3 molecular beam with an initial velocity of 340 m/s is firstly loaded into the electric lattice. Subsequently the packets of molecules in arrays of microtraps are brought to a standstill by the 5-cm-long 2D electric lattice in about 0.3 ms. With the same acceleration of -1.16 μm· μs^{-2}, the molecular packets in the lattice are then shifted back over the chip. In our numerical calculations, the detection laser is perpendicular to the molecular beam axis and transversely passes through each array of packets. As a consequence, there are eleven peaks identified in the 11×11 array for each snapshot, where the spatial interval between each snapshot is $2L/3$ (120 μm) as shown in Fig. 6. The size of the molecular array is limited by the initial emittance of the molecular beam, which is set to relatively small values in our simulation due to the memory limits of the personal computers. In Fig. 6, five typical snapshots record the process during which arrays of packets are shuttled back and forth. Fig. 6(a)–(c) depict the process of stopping the ND_3 molecular packets near the end of the chip. During this process the velocity of the lattice is gradually reduced to zero. Fig. 6(c)–(e) shows that the molecular packets are then shifted back from a stationary state. Evidently, the lattice allows arrays of molecular packets for shuttling back and forth with a smooth manner. The lattice therefore can act as a memory register that contains arrays of cold polar molecules, and qubits are encoded into the internal energy levels of polar molecules [20,25].

5.2. Co-deceleration and co-trapping of two molecular samples

Simultaneous deceleration of two species of molecules that are confined in the same traps permits reducing their overall kinetic energies while canceling their relative velocities in a moving frame of reference, which opens up the pathway to study the sympathetic cooling of two molecular species as well as bimolecular collisions. The Narevicius group utilized merged supersonic molecular beams, which propagate in the same direction such that their relative velocity vanishes, to investigate Penning ionization reactions [27] and isotope effect [26] in cold temperatures. More recently, they produced cold mixtures of atoms and molecules by simultaneously decelerating [10] and trapping [11] oxygen molecules and atoms, using a 2.4-meter long moving magnetic trap decelerator, paving the way towards the sympathetic cooling of molecules. The Ye group studied cold OH (hydroxyl radical)–ND_3 dipolar collisions in a magnetic trap [28], where the two species of samples are produced from Stark decelerator and buffer gas cooling, respectively. However, little work has been done on co-deceleration and co-trapping of two molecular species to date. Here we choose

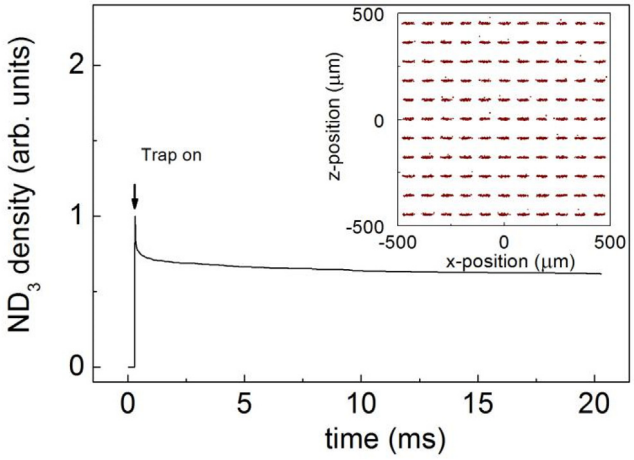

Fig. 5. Directly decelerating a supersonic ND_3 beam to a standstill and trapping them for over twenty milliseconds. The inset shows the 2D view of the molecular distribution in the lattice, which approach towards the end of the chip with a forward velocity being close to zero and are patterned with an 11×11 array in the x-z plane.

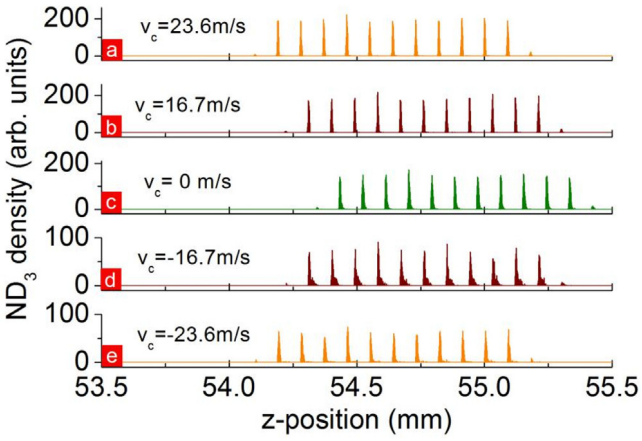

Fig. 6. Shuttling back and forth arrays of ND_3 molecules in the 2D electric lattice. Subpanels (a)–(c) are the snapshots recording the stopping process of the packets, followed by the shifting back of the molecules (subpanels (c)–(e)). The interval between each snapshot is 120 μm (2L/3). The velocities of the lattice are indicated in each panel. The origin of the z-axis is set at the position of the skimmer placed 5 mm before the chip.

ND_3 and CH as a prototype of two molecular species to verify their possibility of Stark deceleration on a chip.

CH is one of the simplest free radicals and widely investigated in astronomical sources, combustion systems and atmospheric applications, as well as in measuring the precision spectroscopy of its Λ-doublet transitions due to its sensitivity to the changes of the fine-structure constant α and so forth [29]. CH is also a good candidate for Stark deceleration with mass to electric moment ratio of 8.9 amu/Debye. The Stark shifts of CH and ND_3 molecules in their electronic and vibrational ground states are shown in Fig. 7(a). Monte-Carlo simulation of co-deceleration of the two molecular samples is carried out with the same parameters used in the above section, where ND_3 molecules in $|J = 1, KM = -1>$ state and CH molecules in $|\ ^2\Pi_{3/2}, J = 3/2, M\Omega = -9/4>$ state are adopted. The two molecular species have the same initial molecular number of 2×10^6, which are simultaneously coupled into the 2D lattice. The amplitudes of the voltages U_1 and U_2 applied on the electrodes are both 100 V, while the frequency of the voltages is continuously chirped from 3.78 MHz to 0 Hz. Same as before, the lattice moves with an acceleration of -1.16 μm· μs^{-2}. After passing through the 5-cm-long molecular chip, the two molecular packets are

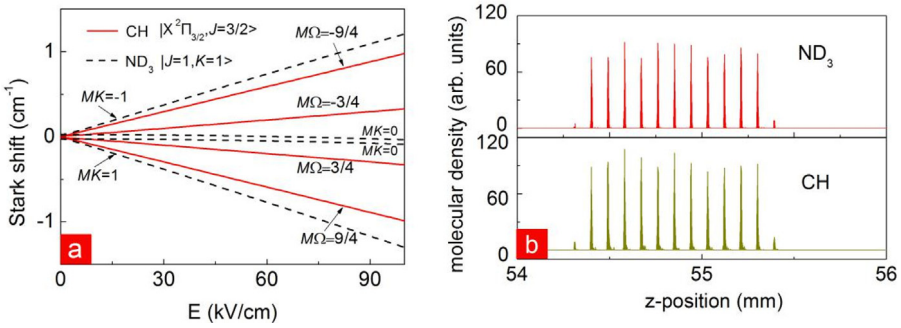

Fig. 7. (a) Stark shifts of ND_3 in $|J = 1, K=1>$ state (dashed lines) and CH in $|X^2\Pi_{3/2}, J=3/2>$ state (solid lines) in an electric field of up to 100 kV/cm, where the splitting is 0.053 cm^{-1} for ND_3 and 0.023 cm^{-1} for CH [26], respectively. (b) Calculated results of simultaneous deceleration of ND_3 (top panel of (b)) and CH (bottom panel of (b)) molecules via the 2D moving electric lattice on a chip.

simultaneously decelerated to rest from an initial velocity of 340 m/s. Fig. 7(b) records the snapshot that the two species are close to the end of the chip, with the same final central velocity approaching zero. We notice that the molecular number of the resulting CH packets is greater than ND_3 by about 50%, due to that the Stark-shift-to-mass ratio of CH is larger than ND_3. These results indicate the possibility of co-deceleration and co-trapping of two molecular samples by our 2D moving electric lattice on a chip,thus providing a comprehensive platform for sympathetic cooling or cold molecular collisions.

6. Conclusions

We have proposed a 2D moving electric lattice on a chip for polar molecules, which is composed of arrays of equidistant electrodes with cosine-modulated voltages. The velocity of these microtraps can be easily controlled by tuning the parameters of the voltages applied on the electrodes, and the distance of the potential minima from the chip remains constant while moving. Theoretical analysis and Monte-Carlo simulations are both set out to attest the feasibility of such a 2D moving electrical lattice via polar molecules of ND_3 and CH. Comparing to the current magnetic or optical lattices with a low trap depth, the electric lattice exhibits a large force, and is capable of stopping supersonic molecular packets in a distance of a few centimeters and shuttling them back and forth over the chip, which in fact overcomes the difficulty in efficiently loading of the microtraps in the optical and magnetic lattices. At last, the electric lattice also enables bringing two molecular species to rest simultaneously from supersonic speeds.

The 2D moving electric lattice provides an innovative means of manipulating and trapping polar molecules. Apart from acting as a molecular shift register for QIP, the lattice can also offer a platform for producing arrays of ultracold polar molecules on a chip with the help of, for instance, adiabatic cooling [30,31], Sisyphus cooling [32] or evaporative cooling [33]. The lattice may also find applications in the study of the interaction between molecules or molecule-surface interaction, novel quantum mechanical collision and cold chemistry on a chip, as well as some other possible applications amenable to magnetic or optical lattices.

CRediT authorship contribution statement

Bin Wei: Software, Writing - original draft. **Hengjiao Guo:** Data curation, Writing - original draft. **Yabing Ji:** Investigation, Formal analysis. **Tao Yang:** Writing - review & editing. **Shunyong Hou:** Conceptualization, Software, Writing - review & editing, Supervision. **Jianping Yin:** Supervision, Project administration, Funding acquisition.

Declaration of competing interest

The authors declare that they have no known competing financial interests or personal relationships that could have appeared to influence the work reported in this paper.

Acknowledgments

This work is supported by the National Nature Science Foundation of China (Grants Numbers 11834003, 91536218, 11034002, 11274114, 11504112, and 11874151); the National Key Basic Research and Development Program of China (2011CB921602), and the Fundamental Research Funds for the Central Universities, Shanghai Pujiang Talents Plan (18PJ1403100), Exploration Funds for the Shanghai Natural Science Foundation, China (18ZR1412700), and the Program for Professor of Special Appointment (Eastern Scholar) at Shanghai Institutions of Higher Learning.

References

[1] A. Negretti, P. Treutlein, T. Calarco, Quantum computing implementations with neutral particles, Quantum Inf. Process. 10 (2011) 721, http://dx.doi.org/10.1007/s11128-011-0291-5.
[2] Y. Miroshnychenko, W. Alt, I. Dotsenko, L. Förster, M. Khudaverdyan, D. Meschede, D. Schrader, A. Rauschenbeutel, An atom-sorting machine, Nature 442 (2006) 151, http://dx.doi.org/10.1038/442151a.
[3] S. Bergamini, B. Darquié, M. Jones, L. Jacubowiez, A. Browaeys, P. Grangier, Holographic generation of microtrap arrays for single atoms by use of a programmable phase modulator, J. Opt. Soc. Amer. B 21 (2004) 1889–1894, http://dx.doi.org/10.1364/JOSAB.21.001889.
[4] R. Dumke, M. Volk, T. Müther, F.B.J. Buchkremer, G. Birkl, W. Ertmer, Micro-optical realization of arrays of selectively addressable dipole traps: a scalable configuration for quantum computation with atomic qubits, Phys. Rev. Lett. 89 (2002) 097903, http://dx.doi.org/10.1103/PhysRevLett.89.097903.
[5] S. Whitlock, R. Gerritsma, T. Fernholz, R.J.C. Spreeuw, Two-dimensional array of microtraps with atomic shift register on a chip, New J. Phys. 11 (2009) 023021, http://dx.doi.org/10.1088/1367-2630/11/2/023021.
[6] S.A. Meek, H.L. Bethlem, H. Conrad, G. Meijer, Trapping molecules on a chip in traveling potential wells, Phys. Rev. Lett. 100 (2008) 153003, http://dx.doi.org/10.1103/PhysRevLett.100.153003.
[7] S.A. Meek, H. Conrad, G. Meijer, Trapping molecules on a chip, Science 324 (2009) 1699–1702, http://dx.doi.org/10.1126/science.1175975.
[8] S.D. Hogan, P. Allmendinger, H. Saßmannshausen, H. Schmutz, F. Merkt, Surface-electrode rydberg-stark decelerator, Phys. Rev. lett. 108 (2012) 063008, http://dx.doi.org/10.1103/PhysRevLett.108.063008.
[9] S. Hou, B. Wei, L. Deng, J. Yin, Chip-based microtrap arrays for cold polar molecules, Phys. Rev. A 96 (2017) 063416, http://dx.doi.org/10.1103/PhysRevA.96.063416.
[10] N. Akerman, M. Karpov, L. David, E. Lavert-Ofir, J. Narevicius, E. Narevicius, Simultaneous deceleration of atoms and molecules in a supersonic beam, New J. Phys. 17 (2015) 065015, http://dx.doi.org/10.1088/1367-2630/17/6/065015.
[11] N. Akerman, M. Karpov, Y. Segev, N. Bibelnik, J. Narevicius, E. Narevicius, Trapping of molecular oxygen together with Lithium atoms, Phys. Rev. Lett. 119 (2017) 073204, http://dx.doi.org/10.1103/PhysRevLett.119.073204.
[12] S.A. Meek, A Stark Decelerator on a Chip (Ph.D. thesis), Freie Universität Berlin, 2010.
[13] S.A. Meek, H. Conrad, G. Meijer, A stark decelerator on a chip, New J. Phys. 11 (2009) 055024, http://dx.doi.org/10.1088/1367-2630/11/5/055024.
[14] S.A. Meek, G. Santambrogio, B.G. Sartakov, H. Conrad, G. Meijer, Suppression of nonadiabatic losses of molecules from chip-based microtraps, Phys. Rev. A 83 (2011) 033413, http://dx.doi.org/10.1103/PhysRevA.83.033413.
[15] S.Y. Buhmann, M.R. Tarbutt, S. Scheel, E.A. Hinds, Surface-induced heating of cold polar molecules, Phys. Rev. A 78 (2008) 052901, http://dx.doi.org/10.1103/PhysRevA.78.052901.

[16] G. Scoles, Atomic and Molecular Beam Methods, Oxford University Press, New York, 1986, p. 27.
[17] M. Gupta, D. Herschbach, A mechanical means to produce intense beams of slow molecules, J. Phys. Chem. A 103 (1999) 10670–10673, http://dx.doi.org/10.1021/jp993560x.
[18] W. Hänsel, J. Reichel, P. Hommelhoff, T.W. Hänsch, Magnetic conveyor belt for transporting and merging trapped atom clouds, Phys. Rev. Lett. 86 (2001) 608–611, http://dx.doi.org/10.1103/PhysRevLett.86.608.
[19] T. Middelmann, S. Falke, C. Lisdat, U. Sterr, Long-range transport of ultracold atoms in a far-detuned one-dimensional optical lattice, New J. Phys. 14 (2012) 073020, http://dx.doi.org/10.1088/1367-2630/14/7/073020.
[20] D. DeMille, Quantum computation with trapped polar molecules, Phys. Rev. Lett. 88 (2002) 067901, http://dx.doi.org/10.1103/PhysRevLett.88.067901.
[21] S.F. Yelin, K. Kirby, R. Côté, Schemes for robust quantum computation with polar molecules, Phys. Rev. A 74 (2006) 050301, http://dx.doi.org/10.1103/PhysRevA.74.050301.
[22] A. André, D. DeMille, J.M. Doyle, M.D. Lukin, S.E. Maxwell, P. Rabl, R.J. Schoelkopf, P. Zoller, A coherent all-electrical interface between polar molecules and mesoscopic superconducting resonators, Nat. Phys. 2 (2006) 636–642, http://dx.doi.org/10.1038/nphys386.
[23] E. Kuznetsova, R. Côté, K. Kirby, S.F. Yelin, Analysis of experimental feasibility of polar-molecule-based phase gates, Phys. Rev. A 78 (2008) 012313, http://dx.doi.org/10.1103/PhysRevA.78.012313.
[24] P. Rabl, D. DeMille, J.M. Doyle, M.D. Lukin, R.J. Schoelkopf, P. Zoller, Hybrid quantum processors: molecular ensembles as quantum memory for solid state circuits, Phys. Rev. Lett. 97 (2006) 033003, http://dx.doi.org/10.1103/PhysRevLett.97.033003.
[25] L.D. Carr, D. DeMille, R.V. Krems, J. Ye, Cold and ultracold molecules: science, technology and applications, New J. Phys. 11 (2009) 05504, http://dx.doi.org/10.1088/1367-2630/11/5/055049.
[26] E. Lavert-Ofir, Y. Shagam, A.B. Henson, S. Gersten, J. Kłos, P.S. Zuchowski, J. Narevicius, E. Narevicius, Observation of the isotope effect in sub-kelvin reactions, Nature Chem. 6 (2014) 332–335, http://dx.doi.org/10.1038/nchem.1857.
[27] A.B. Henson, S. Gersten, Y. Shagam, J. Narevicius, E. Narevicius, Observation of resonances in penning ionization reactions at sub-Kelvin temperatures in merged beams, Science 338 (2012) 234–238, http://dx.doi.org/10.1126/science.1229141.
[28] B.C. Sawyer, B.K. Stuhl, M. Yeo, T.V. Tscherbul, M.T. Hummon, Y. Xia, J. Kłos, D. Patterson, J.M. Doyle, J. Ye, Cold heteromolecular dipolar collisions, Phys. Chem. Chem. Phys. 13 (2011) 19059–19066, http://dx.doi.org/10.1039/c1cp21203f.
[29] S. Truppe, R.J. Hendricks, S.K. Tokunaga, H.J. Lewandowski, M.G. Kozlov, C. Henkel, E.A. Hinds, M.R. Tarbutt, A search for varying fundamental constants using hertz-level frequency measurements of cold CH molecules, Nature Commun. 4 (2013) 2600, http://dx.doi.org/10.1038/ncomms3600.
[30] P. Jansen, M. Quintero-Pérez, T.E. Wall, J.E. van den Berg, S. Hoekstra, H.L. Bethlem, Deceleration and trapping of ammonia molecules in a traveling-wave decelerator, Phys. Rev. A 88 (2013) 043424, http://dx.doi.org/10.1103/PhysRevA.88.043424.
[31] M. Quintero-Pérez, P. Jansen, T.E. Wall, J.E. van den Berg, S. Hoekstra, H.L. Bethlem, Static trapping of polar molecules in a traveling wave decelerator, Phys. Rev. Lett. 110 (2013) 133003, http://dx.doi.org/10.1103/PhysRevLett.110.133003.
[32] M. Zeppenfeld, B.G.U. Englert, R. Glöckner, A. Prehn, M. Mielenz, C. Sommer, L.D. van Buuren, M. Motsch, G. Rempe, Sisyphus cooling of electrically trapped polyatomic molecules, Nature 491 (2012) 570–573, http://dx.doi.org/10.1038/nature11595.
[33] J. Märkle, A.J. Allen, P. Federsel, B. Jetter, A. Günther, J. Fortágh, N.P. Proukakis, T.E. Judd, Evaporative cooling of cold atoms at surfaces, Phys. Rev. A 90 (2014) 023614, http://dx.doi.org/10.1103/PhysRevA.90.023614.